

Dark Recipe for the First Giants: From Population III Stars to Early Supermassive Black Holes via Dark Matter Capture

Sulagna Bhattacharya  ^{1,*} Debajit Bose  ^{2,†} Basudeb Dasgupta  ^{1,‡}
 Jaya Doliya  ^{2,§} and Ranjan Laha  ^{2,¶}

¹ *Tata Institute of Fundamental Research, Homi Bhabha Road, Mumbai 400005, India*

² *Centre for High Energy Physics, Indian Institute of Science,
 C. V. Raman Avenue, Bengaluru 560012, India*

(Dated: January 1, 2026)

The presence of supermassive black holes (SMBHs) at high redshifts ($z > 5$), as revealed by James Webb Space Telescope (JWST), challenges standard black hole (BH) formation scenarios. We propose a mechanism in which non-annihilating dark matter (DM) with non-gravitational interactions with the Standard Model (SM) particles accumulates inside Population III (Pop III) stars, inducing their premature collapse into BH seeds having the same mass as the parent star. Owing to their early formation, these seeds can accrete for longer periods and grow into the SMBHs observed at early cosmic times. Focusing on spin-dependent (SD) DM–proton interactions, we identify regions of parameter space that account for the observed high-redshift SMBH population, their mass function, and the SMBH–stellar mass relation. Portions of this parameter space are testable by forthcoming direct detection experiments. The scenario may lead to distinctive gravitational wave (GW) signatures from SMBH mergers, accessible to Laser Interferometer Space Antenna (LISA) and pulsar timing array (PTA) observations.

INTRODUCTION

Understanding the origin of SMBHs in the early Universe remains a central open problem in cosmology. Optical and infrared surveys, such as the Sloan Digital Sky Survey (SDSS) [1, 2], Canada-France High-redshift Quasar Survey (CFHQS) [3, 4], Subaru High-z Exploration of Low-Luminosity Quasars (SHELLQs) [5], and X-ray observatories like Chandra [6] and eROSITA [7] have discovered SMBHs at redshifts $z \gtrsim 5$ [8]. Additionally, JWST is discovering SMBHs at high redshifts at a remarkable pace [6, 9–11]. JWST has also revealed a new population of red-tinted cosmological sources, known as Little Red Dots (LRDs) [12–20], that are believed to potentially host SMBHs at their centers that are in the early phases of active galactic nuclei (AGN) activity. The characteristic red-tint has been hypothesized to be attributed to the dense dust outflows from these young AGNs that enshroud the central region and significantly redden the emitted light [21–34]. Explaining the rapid assembly of such massive objects poses a key theoretical challenge.

Several pathways have been proposed for the formation of SMBHs at high redshifts. (i) One of the astrophysical scenarios involves remnants of the first generation of stars, i.e., Pop III stars. These metal-free stars are expected to form within dark matter halos of mass $M_{\text{halo}} \gtrsim 10^5\text{--}10^6 M_{\odot}$ at $z \sim 15\text{--}30$, where

baryonic matter can cool efficiently through molecular H_2 transitions to form these stars [35–40]. Heavier Pop III stars ($M_s \gtrsim 260 M_{\odot}$) can collapse directly into BHs of similar mass, which can then accrete to form SMBHs [41]. (ii) Metals expelled from Pop III stars enrich gas clouds, inducing fragmentation and formation of low-mass stars. These stars, formed in dense stellar clusters, undergo repeated collisions to form heavier stars that can collapse into BHs with masses $\mathcal{O}(10^2\text{--}10^3) M_{\odot}$ at $z \sim 10\text{--}20$ [42–47]. (iii) Direct collapse of metal-free gas clouds in the early Universe can form massive BHs with masses $\mathcal{O}(10^4\text{--}10^6) M_{\odot}$ at $z \sim 8\text{--}17$ [48–55]. Different beyond the Standard Model (BSM) frameworks have been proposed that can provide the additional Lyman–Werner (LW) photon background to accelerate the collapse of pristine gas clouds [56–64]. SMBH formation via self-interacting DM, primordial black holes, dark stars, and several other mechanisms have also been studied [65–99].

We explore the scenario where non-annihilating DM particles (e.g., asymmetric DM [100, 101]) scatter non-gravitationally with Pop III star to get captured and accumulate sufficiently to trigger tiny BH formation inside the stellar core [102, 103], which can subsequently accrete the stellar material to form seed of mass $M_{\text{seed}} \sim \mathcal{O}(10\text{--}100) M_{\odot}$. We first try to explain the observed SMBHs ($\gtrsim 10^6 M_{\odot}$) at $z_{\text{obs}} \gtrsim 5$ along with the estimation of the host galaxy stellar mass for an allowed benchmark point of the DM parameter space. For the same benchmark point, we also calculate the SMBH mass function at observed redshifts. Furthermore, we study the associated GWs formed from these isolated SMBH mergers and the stochastic background and their detectability with LISA [104] and PTAs [105].

*S.B., D.B., and J.D. contributed equally to this work.

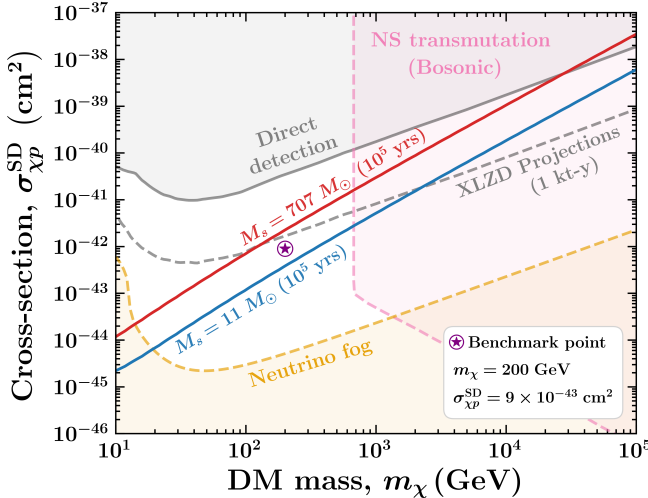


FIG. 1: Contours of seed BH formation time of 10^5 yrs for the lowest (blue) and the highest (red) mass Pop III stars for DM–proton SD interaction ($\sigma_{\chi p}^{\text{SD}}$) are shown along with competitive limits in the parameter space. These two masses represent the lowest and highest masses across all redshifts from [36]. The gray, pink, and orange shaded regions represent the exclusion limits from combined PICO-60 [106] and LZ [107], bounds from neutron star transmutation [108], and the neutrino fog [109], respectively. The purple point denotes the chosen DM benchmark point. The gray dashed curve represents the projected 1 ktonne-year (kt-y) SD sensitivity of XLZD [110], obtained by scaling the current SD LZ limits.

SMBH FORMATION

DM particles (χ) can scatter with SM constituents of Pop III stars and lose sufficient energy to get captured without being evaporated away, provided their mass $m_\chi \gtrsim 10$ GeV [102, 111]. We consider the optically thin regime, which makes the single-scatter approximation valid. The total timescale to form the SMBH seed through DM capture is

$$\tau = \tau_{\text{accum}} + \tau_{\text{therm}} + \tau_{\text{col}} + \tau_{\text{Bondi}}, \quad (1)$$

where τ_{accum} is the accumulation timescale for DM to trigger the collapse, which is determined by $m_\chi C_\chi \tau_{\text{accum}} = \max[M_{\text{self}}, M_{\text{Ch}}]$, with C_χ being the DM capture rate. Here, M_{self} is the self-gravitating mass and M_{Ch} is the Chandrasekhar mass arising from Fermi degeneracy pressure. For bosonic DM, the balancing quantum pressure comes from the zero-point energy of the quantum states or from self-interaction (if it exists) [112–114]. For the considered DM masses, M_{self} overwhelms the degeneracy and quantum pressure of fermionic and bosonic DM, respectively, which makes τ_{accum} and, consequently, the whole framework applicable to both. The thermalization time is denoted by τ_{therm} . The timescale over which

the DM core contracts down to the Schwarzschild radius (r_{Sch}) is denoted by τ_{col} , and τ_{Bondi} is the time required for the tiny BH to consume the parent star via Bondi accretion [115]. Note that, for the parameter space of our interest, the seed formation timescale is dominated by the thermalization timescale. Therefore, the nature of accretion for stellar consumption does not matter much. For our chosen DM parameters, the tiny BH evaporation is negligible [102]. To calculate the capture rate and the associated timescales, we use the properties of Pop III stars obtained from MESA [116–121]. All calculational details are outlined in the *Supplemental Material*.

In Fig. 1, we show the isochrones, contours of the same BH-seed formation time, of $\tau = 10^5$ yrs ($\ll \tau_{\text{PopIII}}$) for the lowest ($11 M_\odot$, $1.5 R_\odot$, $\tau_{\text{lifetime}} = 14.5$ Myr) and the highest Pop III masses ($707 M_\odot$, $16.4 R_\odot$, $\tau_{\text{lifetime}} = 1.9$ Myr) from [36] for SD DM–proton scattering. The purple point corresponds to the considered benchmark parameters ($m_\chi = 200$ GeV, $\sigma_{\chi p}^{\text{SD}} = 9 \times 10^{-43}$ cm 2) that evade existing constraints. Although we present only one benchmark point, Fig. 1 shows that a broader parameter space, including some regions within the neutrino fog, leads to similar τ . Some portions of the allowed DM parameter space can be probed by the XLZD experiment [110]. We also explore whether DM–electron scattering can explain these SMBH observations (see the *Supplemental Material*).

For a Pop III star forming at $z_{\text{in}}(t_{\text{in}})$, the seed BH forms at $z_{\text{seed}}(t_{\text{seed}} = t_{\text{in}} + \tau)$. The seed BH grows via accretion, as defined in Eq. (2). We consider three growth rates: Eddington, sub-Eddington, and super-Eddington. The corresponding Salpeter time is $t_{\text{Sal}} \approx \left(\frac{\epsilon_r}{0.1}\right) 45.1$ Myr [137], where the radiative efficiency ϵ_r is taken to be 0.1 that depends on the BH angular momentum [138]. Our choice of Bondi accretion for stellar consumption by the tiny BH is conservative; however, the subsequent (super-/sub-) Eddington accretion rate for seed BH growth is demanded by the requirement to explain the observational data. With the Bondi accretion rate, a $100 M_\odot$ seed will need a boost factor of $\sim 10^4$ in the ambient halo matter density. The observed BH mass at an observed redshift, $z_{\text{obs}}(t_{\text{obs}})$, is

$$M_{\text{BH}}^{\text{obs}} = M_{\text{Seed}} \times \exp \left[\frac{\eta_{\text{acc}}(1 - \epsilon_r)(t_{\text{obs}} - t_{\text{seed}})}{t_{\text{Sal}}} \right], \quad (2)$$

where η_{acc} denotes the accretion efficiency, taken to be 1.0 for Eddington accretion, 0.5 and 0.75 for sub-Eddington accretion, and 1.4 for super-Eddington growth. In Fig. 2a, we show the observed SMBH masses predicted in our framework as a function of z_{obs} . Each band corresponds to a different accretion efficiency obtained for four initial Pop III formation redshifts, z_{in} , (16, 20, 24, and 28) [36]. The upper and lower edges of each band correspond to

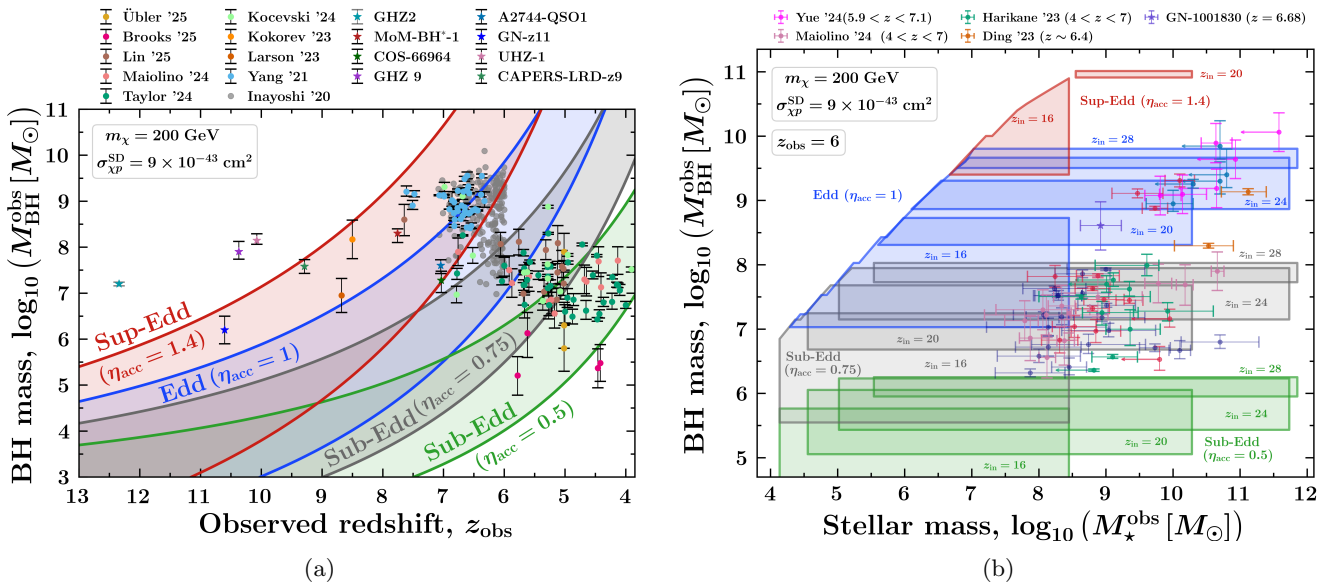


FIG. 2: **Left:** SMBH masses as a function of observed redshifts for our chosen DM benchmark point, shown for Eddington (blue: $\eta_{\text{acc}} = 1$), sub-Eddington (green: $\eta_{\text{acc}} = 0.5$ and gray: $\eta_{\text{acc}} = 0.75$), and super-Eddington (red: $\eta_{\text{acc}} = 1.4$) accretion rates, along with observed SMBHs [8–10, 122–131]. **Right:** SMBH mass and host galaxy stellar mass relation at $z_{\text{obs}} = 6$ is shown for Eddington (blue, $\eta_{\text{acc}} = 1$), sub-Eddington (green: $\eta_{\text{acc}} = 0.5$ and gray: $\eta_{\text{acc}} = 0.75$), and super-Eddington (red: $\eta_{\text{acc}} = 1.4$) accretion rates, together with the observed SMBH and stellar mass data at similar redshifts [127, 132–136].

the heaviest Pop III star at $z = 28$ and the lightest Pop III star at $z = 16$, respectively. For comparison, we overlay the observed SMBHs [8–10, 122–131]. Eddington and sub-Eddington accretion together can explain $\sim 81\%$ of the observed data, which increases to $\sim 99\%$ when super-Eddington accretion is included.

SMBH MASS FUNCTION

The mechanism of DM capture within Pop III stars offers a plausible explanation for the observed SMBHs. We evaluate the SMBH mass function ($\Phi_{\text{BH}}^{\text{obs}}$) by modeling the DM halos and the Pop III star distribution at high redshifts. We consider halo masses spanning $M_{\text{halo}} \in [10^6, 10^9] M_{\odot}$ to ensure the formation of Pop III stars within these halos. The density profile of DM is considered to follow the generalized Navarro–Frenk–White (gNFW) profile [139–141] with an inner slope of $3/2$ [142]. We assume a conservative value for the concentration parameter $c_{200} = 2$ based on Fig. 7 of [143], which shows the dependence of c_{200} on halo masses up to $z = 20$, with typical values of $c_{200} \gtrsim 3$.

We assume one Pop III star at the central region of each halo (at r_{dis}), where the DM density is 10^{11} GeV/cm^3 . The mass of the star is drawn from [36]. Throughout the lifetime of the Pop III star, we assume that it does not migrate too much from this location. At r_{dis} , the rotational and escape velocities of the halos are calculated to evaluate

the DM capture rate (see Section S4). For a given halo mass at z_{in} , we compute τ with the chosen benchmark parameters for each bin of the IMF constructed from [36], followed by four accretion scenarios of the seed BH. With the fitting relation given in [144], we calculate the evolved halo mass at z_{obs} and impose $M_{\text{halo}}^{\text{obs}} \leq M_{\text{halo}}^{\text{obs}}$. This process is carried out for $M_{\text{halo}} \in [10^6, 10^9] M_{\odot}$ for the four chosen z_{in} and then summed at z_{obs} . After tracing the evolution of halo masses up to z_{obs} , the stellar mass of the halos (M_{\star}^{obs}) is obtained by multiplying the DM halo mass by the stellar-to-halo mass fraction derived from the fitting of the Data Release 1 of the UniverseMachine code [145]. For $M_{\text{halo}} < 10^{10.5} M_{\odot}$, where the fractions are unavailable, we adopted the lowest quoted value from the fitting. We plot the obtained stellar mass versus SMBH mass in Fig. 2b at $z_{\text{obs}} = 6$, along with the observations at similar redshifts [127, 132–136]. Collectively, Eddington and sub-Eddington accretion formalisms explain most of the observed data. Increasing observational exploration of high redshifts galaxies such as Abell 2744-QSO1 (at $z_{\text{obs}} = 7$), which exhibit a high SMBH-to-galaxy stellar mass ratio, can provide a unique signature of our scenario.

We derive the SMBH mass function by counting the number of SMBHs in a certain bin multiplied by the comoving number density of halos calculated with the `hmf` code [146, 147]. In Fig. 3, we present the SMBH mass function for z_{obs} of 6 and 6.5 calculated with the benchmark parameters. We have to use a normalization

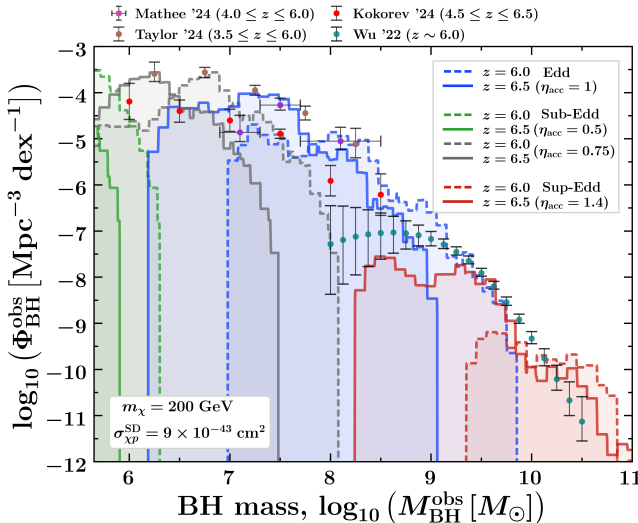


FIG. 3: SMBH mass function calculated at $z_{\text{obs}} = 6.0$ (dashed) and $z_{\text{obs}} = 6.5$ (solid) for Eddington (blue: $\eta_{\text{acc}} = 1$), sub-Eddington (green: $\eta_{\text{acc}} = 0.5$ and gray: $\eta_{\text{acc}} = 0.75$), and super-Eddington (red: $\eta_{\text{acc}} = 1.4$) accretion rates, with the normalization factor (f_{norm}) equal to $10^{-5.9}$, $10^{-5.6}$, $10^{-6.3}$, and $10^{-6.8}$, respectively. Measurements of the SMBH mass function at similar redshifts [13, 150–152] are also displayed.

factor ($f_{\text{norm}} < 1$) in order to match the observations. The f_{norm} can be a product of: (i) the fraction of halos that have a gNFW profile, (ii) the fraction of halos that host Pop III star at the center, and (iii) the fraction of SMBHs that are in their active phase (f_{duty}) [148, 149]. In Fig. 3, we compare our predicted SMBH mass function with the observational results from [13, 150–152]. These datasets also include LRDs that are believed to be associated with dust-enshrouded AGNs. We find that most of the observations of early SMBHs and LRDs can be explained by our scenario.

GRAVITATIONAL WAVES FROM SMBH BINARIES

Dormant SMBHs that remain electromagnetically unobserved can generate GW signals: (i) individual SMBH mergers and (ii) stochastic GW background from their mergers. In Fig. 4, we show the typical GW strain from Eddington-accreted symmetric SMBHs for the lowest and highest z_{in} values for an individual merger. The strain is calculated using the frequency domain IMR-PhenomD [153, 154] waveform template, which is calibrated with the numerical relativity simulations, from the pyCBC code [155], along with the sensitivity curves from LISA [104] (obtained using the fitting given in [156, 157]), and μ Ares [158]. Similar GW signatures can also arise for other scenarios (different Pop III star mass, formation and

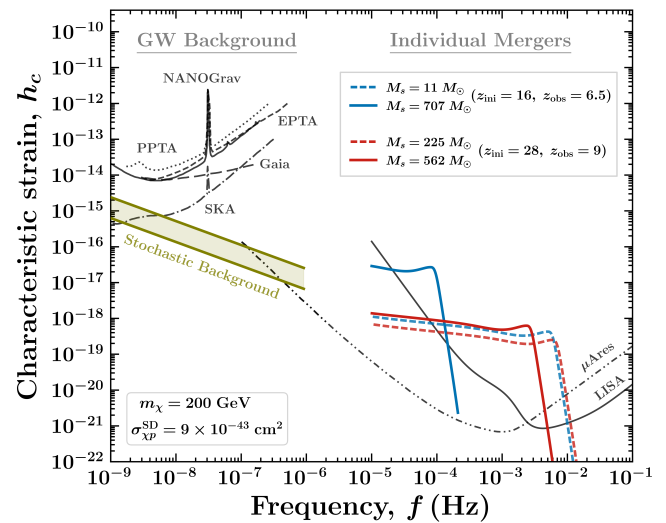


FIG. 4: Characteristic strains from typical SMBH mergers are shown with solid (lowest Pop III mass) and dashed (highest Pop III mass) lines for two values of z_{in} and z_{obs} motivated from the redshift-dependent IMF in [36]. We have evolved seed BHs with Eddington accretion to form SMBHs with masses of $1.5 \times 10^6 M_{\odot}$ (blue, dashed), $9.7 \times 10^7 M_{\odot}$ (blue, solid), $1.3 \times 10^6 M_{\odot}$ (red, dashed), and $3.3 \times 10^6 M_{\odot}$ (red, solid). The stochastic GW background from Eddington-accreting SMBHs is represented by the olive shaded band. The GW detector sensitivities are illustrated with different black lines. The mass ratios for the individual mergers and stochastic background are taken to be 1 and $1/3$, respectively.

observed redshifts, accretion rates, asymmetric mergers) within the LISA and μ Ares sensitivity; however, we have not shown them in Fig. 4 to maintain clarity.

To estimate the stochastic GW background from these SMBH mergers, we follow the approach outlined in [159, 160]. The comoving number density of SMBH mergers is calculated using $n_{\text{SMBH}}^{\text{inspiral}} = n_{\text{SMBH}} \times [\langle \tau_{\text{insp}} \rangle / \langle \tau_{\text{total}} \rangle]$. Here, $\langle \tau_{\text{insp}} \rangle$ is the average inspiral time of the SMBH binary and $\langle \tau_{\text{total}} \rangle$ is the mean total time of the SMBH merger starting from halo coalescence. Their ratio is taken from Table 4 of [160] that compiles results from [161–164]; the differences in the ratio values are reflected in the olive band in Fig. 4. We compute n_{SMBH} by evaluating the Eddington accreted SMBH mass function in the redshift range $z_{\text{obs}} = 10 - 5$ in steps of 0.1. While determining n_{SMBH} , we include an additional factor $f_{\text{other}} = f_{\text{norm}} / f_{\text{duty}}$, where $f_{\text{norm}} = 10^{-5.9}$ (Eddington) and f_{duty} is taken to be 0.1 to remain conservative [148]. This f_{other} includes both active and dormant SMBHs. In Fig. 4, we show the predicted stochastic GW background from these SMBHs, assuming a binary mass ratio of $1/3$, together with the 15-year results from NANOGrav [105]. We also overlay the projected sensitivities from EPTA [165], PPTA [166], Gaia [167], and

SKA [168], as compiled in [169]. Since the average masses of the sub-Eddington accreting BHs lie mostly below the SMBH mass range (see Fig. 2a), we have not shown them. For the super-Eddington case, the GW background nearly overlaps with the Eddington band.

The calculational details for LISA signal-to-noise ratio (SNR) and GW backgrounds are provided in the *Supplemental Material*.

CONCLUSION

The presence of SMBHs and LRDs (assuming an AGN origin) at very high redshifts poses a major challenge for standard astrophysical formation scenarios. While models invoking massive BH seeds can reproduce these observations, generating such seeds in the early Universe is inherently rare. We investigate the premature collapse of Pop III stars induced by the accumulation of non-annihilating DM. Focusing on the SD DM–proton scattering, we identify benchmark cross sections – beyond current DM direct detection limits – that induce BH formation within $\sim 10\%$ of the standard Pop III stellar lifetime.

For the benchmark DM mass and SD DM–proton scattering cross section, our framework can account for the bulk of the observed high-redshift SMBH population when allowing for Eddington, sub-Eddington, and super-Eddington accretion. We compute the SMBH mass function at $z = 6$ and 6.5, finding good agreement with current observations. In estimating the SMBH number density, we follow the evolution of host halos to infer stellar masses and compare the resulting SMBH–stellar mass relation at $z_{\text{obs}} = 6$, which is consistent with the data. The framework further predicts SMBH-to-stellar mass ratios exceeding unity, especially in low-mass galaxies, providing a clear target for upcoming surveys.

Given the substantial population of SMBHs in the early Universe, our framework naturally predicts gravitational-wave signals from both individual mergers and a stochastic background. We find that the strain from individual mergers falls within the projected sensitivity of LISA, and μ Ares, while the associated stochastic background is consistent with the 15-year sensitivity limits reported by the PTA collaboration, and is expected to be probed by SKA in the future.

Taken together, these results highlight a scenario that is necessarily uncertain in its details, but rich in observational consequences. The confluence of data from JWST, DM searches, and GW observatories makes this an especially timely and promising direction to explore.

ACKNOWLEDGMENTS

We sincerely thank Subhadip Bouri, Prolay Chanda, Anirban Das, Raghuvir Garani, Subhajit Ghosh, Shunsaku Horiuchi, Tarak Nath Maity, Ranjini Mondol, Rohan Pramanick, Surjeet Rajendran, Nirmal Raj, Anupam Ray, Akash Kumar Saha, Tracy R. Slatyer, and Gaurav Tomar for their helpful discussions and insightful suggestions. D.B. acknowledges the Council of Scientific and Industrial Research (CSIR), Government of India, for supporting his research under the Research Associateship program through grant no. 09/0079(24106)/2025-EMR-I, and support from the ISRO-IISc STC for the grant no. ISTC/PHY/RL/499. B.D. acknowledges the support of the Dept. of Atomic Energy (Govt. of India) research project RTI 4002, and the Dept. of Science and Technology (Govt. of India) for the Swarna-jayanti Fellowship. R.L. acknowledges financial support from the institute start-up funds, ISRO-IISc STC for the grant no. ISTC/PHY/RL/499, and ANRF for the grant no. ANRF/ARG/2025/005140/PS.

* sulagna@theory.tifr.res.in

† debjitbose550@gmail.com

‡ bdasgupta@theory.tifr.res.in

§ jayadoliya@iisc.ac.in

¶ ranjanlaha@iisc.ac.in

- [1] SDSS collaboration, *A Survey of $z > 5.8$ quasars in the Sloan Digital Sky Survey I: Discovery of three new quasars and the spatial density of luminous quasars at $z \sim 6$* , *Astron. J.* **122** (2001) 2833 [[astro-ph/0108063](#)].
- [2] SDSS collaboration, *A Survey of $z > 5.7$ quasars in the Sloan Digital Sky Survey. 2. Discovery of three additional quasars at $z > 6$* , *Astron. J.* **125** (2003) 1649 [[astro-ph/0301135](#)].
- [3] C. J. Willott et al., *Four quasars above redshift 6 discovered by the Canada-France High- z Quasar Survey*, *Astron. J.* **134** (2007) 2435 [[0706.0914](#)].
- [4] C. J. Willott et al., *The Canada-France High- z Quasar Survey: nine new quasars and the luminosity function at redshift 6*, *Astron. J.* **139** (2010) 906 [[0912.0281](#)].
- [5] Y. Matsuoka, M. A. Strauss, N. Kashikawa, M. Onoue, K. Iwasawa, J.-J. Tang et al., *Subaru high- z exploration of low-luminosity quasars (shellqs). v. quasar luminosity function and contribution to cosmic reionization at $z = 6$* , *The Astrophysical Journal* **869** (2018) 150.
- [6] A. Bogdan et al., *Evidence for heavy-seed origin of early supermassive black holes from a $z \approx 10$ X-ray quasar*, *Nature Astron.* **8** (2024) 126 [[2305.15458](#)].
- [7] P. Medvedev, S. Sazonov, M. Gilfanov, R. Burenin, G. Khorunzhev, A. Meshcheryakov et al., *SRG/eROSITA uncovers the most X-ray luminous quasar at $z > 6$* , *Mon. Not. Roy. Astron. Soc.* **497** (2020) 1842 [[2007.04735](#)].
- [8] K. Inayoshi, E. Visbal and Z. Haiman, *The Assembly of the First Massive Black Holes*, *Ann. Rev. Astron. Astrophys.* **58** (2020) 27 [[1911.05791](#)].

[9] R. Maiolino et al., *A small and vigorous black hole in the early Universe*, *Nature* **627** (2024) 59 [2305.12492].

[10] O. E. Kovacs et al., *A Candidate Supermassive Black Hole in a Gravitationally Lensed Galaxy at $Z \approx 10$* , *Astrophys. J. Lett.* **965** (2024) L21 [2403.14745].

[11] H. Übler, G. Mazzolari, R. Maiolino, F. D'Eugenio, N. Davari, I. Juodžbalis et al., *BlackTHUNDER: evidence for three massive black holes in a $z \sim 5$ galaxy*, *arXiv e-prints* (2025) arXiv:2509.21575 [2509.21575].

[12] I. Labb  , P. G. van Dokkum, E. J. Nelson, R. S. Bezanson, K. A. Suess, J. Leja et al., *A population of red candidate massive galaxies 600 myr after the big bang*, *Nature* **616** (2022) 266.

[13] J. Matthee et al., *Little Red Dots: An Abundant Population of Faint Active Galactic Nuclei at $z \sim 5$ Revealed by the EIGER and FRESCO JWST Surveys*, *Astrophys. J.* **963** (2024) 129 [2306.05448].

[14] V. I. Kokorev, K. I. Caputi, J. E. Greene, P. Dayal, M. Trebitsch, S. E. Cutler et al., *A census of photometrically selected little red dots at $4 < z < 9$ in jwst blank fields*, *The Astrophysical Journal* **968** (2024) .

[15] Z. Zhang, L. Jiang, W. Liu, L. C. Ho and K. Inayoshi, *Just insights into narrow-line little red dots*, 2025, <https://api.semanticscholar.org/CorpusID:279244239>.

[16] K. Ronayne, C. Papovich, A. Kirkpatrick, B. E. Backhaus, F. Cullen, L. Shen et al., *Mega: Spectrophotometric sed fitting of little red dots detected in jwst miri*, 2025, <https://api.semanticscholar.org/CorpusID:280950156>.

[17] T. S. Tanaka, H. B. Akins, Y. Harikane, J. D. Silverman, C. M. Casey, K. Inayoshi et al., *Discovery of a little red dot candidate at $z > 10$ in cosmos-web based on miri-nircam selection*, *The Astrophysical Journal* **995** (2025) 21.

[18] R. Maiolino et al., *A black hole in a near-pristine galaxy 700 million years after the Big Bang*, [2505.22567](https://api.semanticscholar.org/CorpusID:2505.22567).

[19] J. E. Greene et al., *What you see is what you get: empirically measured bolometric luminosities of Little Red Dots*, [2509.05434](https://api.semanticscholar.org/CorpusID:2509.05434).

[20] S. Fu, Z. Zhang, D. Jiang, J. Chen, L. Jiang, L. C. Ho et al., *Discovery of two little red dots transitioning into quasars*, 2025, <https://api.semanticscholar.org/CorpusID:283458496>.

[21] F. Pacucci and R. Narayan, *Mildly Super-Eddington Accretion onto Slowly Spinning Black Holes Explains the X-Ray Weakness of the Little Red Dots*, *Astrophys. J.* **976** (2024) 96 [2407.15915].

[22] A. de Graaff, G. B. Brammer, A. Weibel, Z. J. Lewis, M. V. Maseda, P. A. Oesch et al., *Rubies: A complete census of the bright and red distant universe with jwst/nirspec*, *Astronomy & Astrophysics* (2024) .

[23] K. Ronayne, C. Papovich, A. Kirkpatrick, B. E. Backhaus, F. Cullen, L. Shen et al., *Mega: Spectrophotometric sed fitting of little red dots detected in jwst miri*, 2025.

[24] M.-Y. Zhuang, J. Li, Y. Shen, X. Lin, A. E. Shapley, F. Wang et al., *NEXUS: A Spectroscopic Census of Broad-line AGNs and Little Red Dots at $3 \lesssim z \lesssim 6$* , *arXiv e-prints* (2025) arXiv:2505.20393 [2505.20393].

[25] G. Quadri, A. Trinca, A. Lupi, M. Colpi and M. Volonteri, *Super-Eddington accretion in high-redshift quasar hosts: Black-hole driven outflows, galaxy quenching, and the nature of little red dots*, [2505.05556](https://api.semanticscholar.org/CorpusID:2505.05556).

[26] K. Inayoshi, J. Shangguan, X. Chen, L. C. Ho and Z. Haiman, *The Emergence of Little Red Dots from Binary Massive Black Holes*, [2505.05322](https://api.semanticscholar.org/CorpusID:2505.05322).

[27] I. Juod  balis, C. Marconcini, F. D'Eugenio, R. Maiolino, A. Marconi, H.   bler et al., *A direct black hole mass measurement in a Little Red Dot at the Epoch of Reionization*, *arXiv e-prints* (2025) arXiv:2508.21748 [2508.21748].

[28] S. Kim, W.-S. Jeong, M. Kim, H. D. Jun, Y. Yang and T. Nakagawa, *The bluedog at cosmic noon: A possible analog to little red dots?*, *The Astrophysical Journal* **992** (2025) .

[29] I. Delvecchio, E. Daddi, B. Magnelli, D. Elbaz, M. Giavalisco, A. Traina et al., *Agn-heated dust revealed in "little red dots"*, 2025, <https://api.semanticscholar.org/CorpusID:281217840>.

[30] F. Pacucci, L. Hernquist and M. Fujii, *Little Red Dots are Nurseries of Massive Black Holes*, *Astrophys. J.* **994** (2025) 40 [2509.02664].

[31] B. Jones, D. D. Kocevski, F. Pacucci, A. J. Taylor, S. L. Finkelstein, J. Buchner et al., *The $\$m_{\{bh\}}-m_{\{*\}}$ relationship at $\$3$* , 2025, <https://api.semanticscholar.org/CorpusID:281951104>.

[32] D. Herrero-Carri  n, D. Spinosa, D. Izquierdo-Villalba, T. Su, S. Bonoli and P. Renard, *Back to basics: Little Red Dots as galaxies and dust-obscured AGNs in a synthetic NIRCam sky simulated with L-GalaxiesBH*, *arXiv e-prints* (2025) arXiv:2511.10725 [2511.10725].

[33] A. de Graaff, R. E. Hviding, R. P. Naidu, J. E. Greene, T. B. Miller, J. Leja et al., *Little red dots host black hole stars: A unified family of gas-reddened agn revealed by jwst/nirspec spectroscopy*, 2025, <https://api.semanticscholar.org/CorpusID:283439221>.

[34] K. Inayoshi and L. C. Ho, *A critical evaluation of the physical nature of the little red dots*, 2025, <https://api.semanticscholar.org/CorpusID:283467130>.

[35] S. Hirano, T. Hosokawa, N. Yoshida, H. Umeda, K. Omukai, G. Chiaki et al., *One Hundred First Stars : Protostellar Evolution and the Final Masses*, *Astrophys. J.* **781** (2014) 60 [1308.4456].

[36] S. Hirano, T. Hosokawa, N. Yoshida, K. Omukai and H. W. Yorke, *Primordial star formation under the influence of far ultraviolet radiation: 1540 cosmological haloes and the stellar mass distribution*, *Mon. Not. Roy. Astron. Soc.* **448** (2015) 568 [1501.01630].

[37] R. S. Klessen and S. C. O. Glover, *The First Stars: Formation, Properties, and Impact*, *Ann. Rev. Astron. Astrophys.* **61** (2023) 65 [2303.12500].

[38] M.-Y. Ho, K.-J. Chen and P.-C. Tung, *Turbulence in Primordial Dark Matter Halos and Its Impact on the First Star Formation*, [2505.23768](https://api.semanticscholar.org/CorpusID:2505.23768).

[39] R. S. Ellis, *Galaxies and black holes in the first billion years*, 2025, <https://api.semanticscholar.org/CorpusID:280711670>.

[40] S. C. O. Glover and R. S. Klessen, *The first stars*, 2025, <https://api.semanticscholar.org/CorpusID:281394486>.

[41] M. Sanati, J. C. Tan, J. Devriendt, A. D. Slyz, S. Martin-Alvarez, M. la Torre et al., *The emergence and ionizing feedback of pop iii.1 stars as progenitors for supermassive black holes*, 2025, <https://api.semanticscholar.org/CorpusID:280401094>.

[42] K. Omukai, R. Schneider and Z. Haiman, *Can Supermassive Black Holes Form in Metal-Enriched*

*High-Redshift Protogalaxies ?, *Astrophys. J.* **686** (2008) 801* [0804.3141].

[43] D. Bernadetta and V. Marta, *Formation of massive black hole seeds: runaway collisions in the first stellar clusters*, *Astrophys. J.* **694** (2009) 302 [0810.1057].

[44] A. Rantala and T. Naab, *A rapid channel for the collisional formation and gravitational wave driven mergers of supermassive black hole seeds at high redshift*, *Monthly Notices of the Royal Astronomical Society: Letters* (2025) .

[45] B. Reinoso, M. A. Latif and D. R. G. Schleicher, *Massive black hole formation in population iii star clusters*, *Astronomy & Astrophysics* (2025) .

[46] A. K. Bhowmick, L. Blecha, P. Torrey, L. Z. Kelley, P. Natarajan, R. S. Somerville et al., *Heavy seeds and the first black holes: Insights from the brahma simulations*, 2025, <https://api.semanticscholar.org/CorpusID:281724764>.

[47] A. Dekel, D. D. Chowdhury, S. Lapiner, Z. Yao, S. Gilbaum, D. Ceverino et al., *From feedback-free star clusters to little red dots via compaction*, 2025, <https://api.semanticscholar.org/CorpusID:282921354>.

[48] D. J. Eisenstein and A. Loeb, *Origin of quasar progenitors from the collapse of low spin cosmological perturbations*, *Astrophys. J.* **443** (1995) 11 [astro-ph/9401016].

[49] A. Ferrara, S. Salvadori, B. Yue and D. R. G. Schleicher, *Initial mass function of intermediate mass black hole seeds*, *Mon. Not. Roy. Astron. Soc.* **443** (2014) 2410 [1406.6685].

[50] J. Jeon, V. Bromm, B. Liu and S. L. Finkelstein, *Physical Pathways for JWST-observed Supermassive Black Holes in the Early Universe*, *Astrophys. J.* **979** (2025) 127 [2402.18773].

[51] J. Jeon, B. Liu, A. J. Taylor, V. I. Kokorev, J. Chisholm, D. D. Kocevski et al., *The emerging black hole mass function in the high-redshift universe*, *The Astrophysical Journal* **988** (2025) .

[52] K. Kimura, K. Inayoshi and K. Omukai, *Massive black hole seed formation in strong x-ray environments at high redshift*, *The Astrophysical Journal* **990** (2025) .

[53] E. Cenci and M. Habouzit, *Little red dots as direct-collapse black hole nurseries*, *Monthly Notices of the Royal Astronomical Society* (2025) .

[54] J. Jeon, B. Liu, V. Bromm, S. Fujimoto, A. J. Taylor, V. I. Kokorev et al., *Little red dots and their progenitors from direct collapse black holes*, 2025, <https://api.semanticscholar.org/CorpusID:280691833>.

[55] A. D. Santarelli, C. B. Campbell, E. Farag, E. P. Bellinger, P. Natarajan and M. E. Caplan, *MESA-QUEST: Tracing the formation of direct collapse black hole seeds via quasi-stars*, other thesis, 10, 2025.

[56] A. Friedlander, S. Schon and A. C. Vincent, *Supermassive black hole seeds from sub-keV dark matter*, *JCAP* **06** (2023) 033 [2212.11100].

[57] Y. Lu, Z. S. C. Picker and A. Kusenko, *High-redshift supermassive black holes from tiny black hole explosions*, *Phys. Rev. D* **109** (2024) 123016 [2312.15062].

[58] Y. Lu, Z. S. C. Picker and A. Kusenko, *Direct Collapse Supermassive Black Holes from Relic Particle Decay*, *Phys. Rev. Lett.* **133** (2024) 091001 [2404.03909].

[59] H. Jiao, R. Brandenberger and V. Kamali, *Direct Collapse Supermassive Black Holes from Ultralight Dark Matter*, **2503.19414**.

[60] Y. Lu, Z. Picker, A. Kusenko and T. T. Yanagida, *Neutrino masses, matter-antimatter asymmetry, dark matter, and supermassive black hole formation explained with Majorons*, **2506.23401**.

[61] W. Qin, S. Kumar, P. Natarajan and N. Weiner, *Not-quite-primordial black holes*, **2506.13858**.

[62] L. Zwick, C. Tiede and L. Mayer, *Little Red Dots as self-gravitating discs accreting on supermassive stars: Spectral appearance and formation pathway of the progenitors to direct collapse black holes*, **2507.22014**.

[63] S. Zhang, B. Liu and V. Bromm, *A Novel Formation Channel for Supermassive Black Hole Binaries in the Early Universe via Primordial Black Holes*, *Astrophys. J.* **992** (2025) 136 [2508.00774].

[64] Y. Aggarwal, J. B. Dent, P. Tanedo and T. Xu, *Direct Collapse Black Hole Candidates from Decaying Dark Matter*, **2509.25325**.

[65] S. Balberg, S. L. Shapiro and S. Inagaki, *Selfinteracting dark matter halos and the gravothermal catastrophe*, *Astrophys. J.* **568** (2002) 475 [astro-ph/0110561].

[66] J. Pollack, D. N. Spergel and P. J. Steinhardt, *Supermassive Black Holes from Ultra-Strongly Self-Interacting Dark Matter*, *Astrophys. J.* **804** (2015) 131 [1501.00017].

[67] Y. Lu, Z. S. C. Picker, S. Profumo and A. Kusenko, *Black holes from Fermi ball collapse*, *Phys. Rev. D* **111** (2025) 043005 [2411.17074].

[68] M. G. Roberts, L. Braff, A. Garg, S. Profumo, T. Jeltema and J. O'Donnell, *Early formation of supermassive black holes from the collapse of strongly self-interacting dark matter*, *JCAP* **01** (2025) 060 [2410.17480].

[69] F. Ziparo, S. Gallerani and A. Ferrara, *Primordial black holes as supermassive black hole seeds*, *JCAP* **04** (2025) 040 [2411.03448].

[70] M. R. Buckley and N. Fernandez, *Force-feeding Supermassive Black Holes with Dissipative Dark Matter*, **2410.06252**.

[71] T. Schwemberger and V. Takhistov, *Diffuse Neutrino Signals from Dark Stars Seeding Supermassive Black Holes*, *Astrophys. J. Lett.* **989** (2025) L44 [2412.18654].

[72] F. Jiang, Z. Jia, H. Zheng, L. C. Ho, K. Inayoshi, X. Shen et al., *Formation of the Little Red Dots from the Core-collapse of Self-interacting Dark Matter Halos*, **2503.23710**.

[73] T. Shen, X. Shen, H. Xiao, M. Vogelsberger and F. Jiang, *Massive Black Holes Seeded by Dark Matter – Implications for Little Red Dots and Gravitational Wave Signatures*, **2504.00075**.

[74] M. G. Roberts, L. Braff, A. Garg, S. Profumo and T. Jeltema, *Little Red Dots from Ultra-Strongly Self-Interacting Dark Matter*, **2507.03230**.

[75] S. Li, R. Li, K. Wang, Z. Jia, X. Cao, C. S. Frenk et al., *The "little dark dot": Evidence for self-interacting dark matter in the strong lens sdss j0946+1006?*, 2025, <https://api.semanticscholar.org/CorpusID:277824109>.

[76] V. Tran, X. Shen, D. Gilman, M. Vogelsberger, S. O'Neil, D. Xiong et al., *Core collapse in resonant self-interacting dark matter across two decades in halo mass*, *Phys. Rev. D* **112** (2025) 083003 [2504.02928].

[77] M.-C. Chen and Y. Tang, *Probing self-interacting dark matter via gravitational-wave background from eccentric supermassive black hole mergers*, *Phys. Rev. D* **112** (2025) 043033 [2505.09219].

[78] W.-X. Feng, H.-B. Yu and Y.-M. Zhong, *Dark Bondi Accretion Aided by Baryons and the Origin of JWST Little Red Dots*, [2506.17641](#).

[79] M. Kiyuna, *Super-eddington growth ceiling: Analytic constraints on the rapid growth of light-seed black holes in massive clumps*, *Monthly Notices of the Royal Astronomical Society* (2025) .

[80] L. R. Prole, J. A. Regan, D. Mehta, P. Coles and P. Dayal, *Primordial black holes in cosmological simulations: growth prospects for supermassive black holes*, [2506.11233](#).

[81] P. Dayal and R. maiolino, *The properties of primordially-seeded black holes and their hosts in the first billion years: implications for JWST*, [2506.08116](#).

[82] H. Yajima, *Formation of over-massive black holes in high-redshift disk galaxies via globular cluster accretion*, 2025, <https://api.semanticscholar.org/CorpusID:280391150>.

[83] B. Cyr, *Not-quite-primordial black holes seeded by cosmic string loops*, [2507.17833](#).

[84] J. Mould and A. Batten, *If quasars form from primordial black holes*, 2025, <https://api.semanticscholar.org/CorpusID:280264222>.

[85] B. Zhang, W.-X. Feng and H. An, *Little Red Dots from Small-Scale Primordial Black Hole Clustering*, [2507.07171](#).

[86] M. G. Roberts, L. Braff, A. Garg, S. Profumo and T. E. Jeltema, *Little red dots from ultra-strongly self-interacting dark matter*, 2025, <https://api.semanticscholar.org/CorpusID:280126646>.

[87] D. Nandal, K. Topalakis, J. C. Tan, V. Sergienko, A. Pauchett and M. Petkova, *The Evolution of Pop III.1 Protostars Powered by Dark Matter Annihilation. I. Fiducial model and first results*, [2507.00870](#).

[88] A. Imai, G. J. Mathews, G. Tang and B. Zhang, *Dark Matter and the Early Formation of Supermassive Black Holes*, [2508.11846](#).

[89] X. Dong, Y. Zhu, M. Rieke, G. Rieke, X. Li, P. Behroozi et al., *A Promise for the JWST era: Massive black holes directly collapsed from wave dark matter haloes, and Star formation in and around their accretion flows*, [2508.09258](#).

[90] J. McDonald, *Superheavy Q-Balls and Cosmology*, [2508.08931](#).

[91] Y. Chen, H. Mo and H. Wang, *A two-phase model of galaxy formation: IV. Seeding and growing supermassive black holes in dark matter halos*, [2509.03283](#).

[92] J. Ellis, M. Fairbairn, J. Urrutia and V. Vaskonen, *Constraints on Dark Matter Models from Supermassive Black Hole Evolution*, [2509.06955](#).

[93] K. Kritos and J. Silk, *From nuclear star clusters to Little Red Dots: black hole growth, mergers, and tidal disruptions*, [2510.21709](#).

[94] N. Sanchis-Gual, J. Barranco, J. C. Degollado and D. Nuñez, *Dark-to-black super accretion as a mechanism for early supermassive black hole growth*, [2510.00644](#).

[95] K. Topalakis, D. Nandal and J. C. Tan, *The Evolution of Pop III.1 Protostars Powered by Dark Matter Annihilation. II. Dependence on WIMP Properties*, [2510.00216](#).

[96] C.-S. Chen and F.-L. Lin, *A Unified Dark-Matter-Driven Relativistic Bondi Route to Black-Hole Growth from Stellar to Supermassive Scales*, [2511.09311](#).

[97] C. Ilie, J. Paulin, A. Petric and K. Freese, *Supermassive Dark Stars and their remnants as a possible solution to three recent cosmic dawn puzzles*, [2511.08477](#).

[98] K. Freese, G. M. Fuller, S. Ghodla, C. Ilie, K. S. Kehrer, T. Rindler-Daller et al., *Early Formation of Supermassive Black Holes via Dark Star Gravitational Instability*, [2511.08578](#).

[99] A. Pauchet and D. Nandal, *Dark-matter-powered population iii evolution: Lifetimes, rotation, and quasi-homogeneity in massive stars*, 2025, <https://api.semanticscholar.org/CorpusID:282757904>.

[100] K. Petraki and R. R. Volkas, *Review of asymmetric dark matter*, *Int. J. Mod. Phys. A* **28** (2013) 1330028 [[1305.4939](#)].

[101] K. M. Zurek, *Asymmetric Dark Matter: Theories, Signatures, and Constraints*, *Phys. Rept.* **537** (2014) 91 [[1308.0338](#)].

[102] S. A. R. Ellis, *Premature black hole death of Population III stars by dark matter*, *JCAP* **05** (2022) 025 [[2111.02414](#)].

[103] J. Diks and C. Ilie, *Constraining Asymmetric DM Properties by Black Hole Formation in Neutron Stars and Population III Stars*, [2412.07953](#).

[104] P. Amaro-Seoane, H. Audley, S. Babak, J. Baker, E. Barausse, P. Bender et al., *Laser Interferometer Space Antenna*, *arXiv e-prints* (2017) [[1702.00786](#)].

[105] NANOGrav collaboration, *The NANOGrav 15 yr Data Set: Detector Characterization and Noise Budget*, *Astrophys. J. Lett.* **951** (2023) L10 [[2306.16218](#)].

[106] PICO collaboration, *Dark Matter Search Results from the Complete Exposure of the PICO-60 C₃F₈ Bubble Chamber*, *Phys. Rev. D* **100** (2019) 022001 [[1902.04031](#)].

[107] LZ collaboration, *Dark Matter Search Results from 4.2 Tonne-Years of Exposure of the LUX-ZEPLIN (LZ) Experiment*, *Phys. Rev. Lett.* **135** (2025) 011802 [[2410.17036](#)].

[108] R. Garani, Y. Genolini and T. Hambye, *New Analysis of Neutron Star Constraints on Asymmetric Dark Matter*, *JCAP* **05** (2019) 035 [[1812.08773](#)].

[109] C. A. J. O'Hare, *New Definition of the Neutrino Floor for Direct Dark Matter Searches*, *Phys. Rev. Lett.* **127** (2021) 251802 [[2109.03116](#)].

[110] XLZD collaboration, *The XLZD Design Book: towards the next-generation liquid xenon observatory for dark matter and neutrino physics*, *Eur. Phys. J. C* **85** (2025) 1192 [[2410.17137](#)].

[111] R. Garani and S. Palomares-Ruiz, *Evaporation of dark matter from celestial bodies*, *JCAP* **05** (2022) 042 [[2104.12757](#)].

[112] P.-H. Chavanis and T. Harko, *Bose-Einstein Condensate general relativistic stars*, *Phys. Rev. D* **86** (2012) 064011 [[1108.3986](#)].

[113] N. F. Bell, A. Melatos and K. Petraki, *Realistic neutron star constraints on bosonic asymmetric dark matter*, *Phys. Rev. D* **87** (2013) 123507 [[1301.6811](#)].

[114] J. Eby, C. Kouvaris, N. G. Nielsen and L. C. R. Wijewardhana, *Boson Stars from Self-Interacting Dark Matter*, *JHEP* **02** (2016) 028 [[1511.04474](#)].

[115] H. Bondi, *On spherically symmetrical accretion*, *Mon. Not. Roy. Astron. Soc.* **112** (1952) 195.

[116] MESA collaboration, *Modules for Experiments in Stellar Astrophysics (MESA)*, *Astrophys. J. Suppl.* **192** (2011) 3 [[1009.1622](#)].

[117] B. Paxton, M. Cantiello, P. Arras, L. Bildsten, E. F. Brown, A. L. Dotter et al., *Modules for experiments in stellar astrophysics (mesa): Planets, oscillations, rotation, and massive stars*, *The Astrophysical Journal Supplement Series* **208** (2013) .

[118] B. Paxton, P. Marchant, J. Schwab, E. B. Bauer, L. Bildsten, L. Bildsten et al., *Modules for experiments in stellar astrophysics (mesa): Binaries, pulsations, and explosions*, *The Astrophysical Journal Supplement Series* **220** (2015) .

[119] B. Paxton et al., *Modules for Experiments in Stellar Astrophysics (MESA): Convective Boundaries, Element Diffusion, and Massive Star Explosions*, *Astrophys. J. Suppl.* **234** (2018) 34 [2170.08424].

[120] B. Paxton, R. Smolec, J. Schwab, A. Gautschy, L. Bildsten, L. Bildsten et al., *Modules for experiments in stellar astrophysics (mesa): Pulsating variable stars, rotation, convective boundaries, and energy conservation*, *The Astrophysical Journal Supplement Series* **243** (2019) .

[121] MESA collaboration, *Modules for Experiments in Stellar Astrophysics (MESA): Time-dependent Convection, Energy Conservation, Automatic Differentiation, and Infrastructure*, *Astrophys. J. Suppl.* **265** (2023) 15 [2208.03651].

[122] A. J. Taylor, V. I. Kokorev, D. D. Kocevski, H. B. Akins, F. Cullen, M. Dickinson et al., *Capers-lrd-z9: A gas enshrouded little red dot hosting a broad-line agn at z=9.288*, 2025, <https://api.semanticscholar.org/CorpusID:278368460>.

[123] J. Yang et al., *Probing Early Supermassive Black Hole Growth and Quasar Evolution with Near-infrared Spectroscopy of 37 Reionization-era Quasars at $6.3 < z \leq 7.64$* , *Astrophys. J.* **923** (2021) 262 [2109.13942].

[124] A. D. Goulding et al., *UNCOVER: The Growth of the First Massive Black Holes from JWST/NIRSpec—Spectroscopic Redshift Confirmation of an X-Ray Luminous AGN at $z = 10.1$* , *Astrophys. J. Lett.* **955** (2023) L24 [2308.02750].

[125] R. L. Larson, S. L. Finkelstein, D. D. Kocevski, T. A. Hutchison, J. R. Trump, P. A. Haro et al., *A ceers discovery of an accreting supermassive black hole 570 myr after the big bang: Identifying a progenitor of massive $z \gtrsim 6$ quasars*, *The Astrophysical Journal Letters* **953** (2023) .

[126] V. I. Kokorev, S. Fujimoto, I. Labb  , J. E. Greene, R. S. Bezanson, P. Dayal et al., *Uncover: A nirspecl identification of a broad-line agn at $z = 8.50$* , *The Astrophysical Journal Letters* **957** (2023) .

[127] R. Maiolino et al., *JADES - The diverse population of infant black holes at $4 < z < 11$: Merging, tiny, poor, but mighty*, *Astron. Astrophys.* **691** (2024) A145 [2308.01230].

[128] L. J. Furtak, I. Labb  , A. Zitrin, J. E. Greene, P. Dayal, I. Chemerynska et al., *A high black hole to host mass ratio in a lensed agn in the early universe.*, *Nature* (2023) .

[129] R. P. Naidu et al., *A "Black Hole Star" Reveals the Remarkable Gas-Enshrouded Hearts of the Little Red Dots*, **2503.16596**.

[130] X. Lin, X. Fan, F. Wang, F. Sun, J. B. Champagne, E. Egami et al., *Bridging quasars and little red dots: Insights into broad-line agns at $\$z=5-8\$$ from the first jwst cosmos-3d dataset*, 2025, <https://api.semanticscholar.org/CorpusID:277740732>.

[131] H. B. Akins, C. M. Casey, D. A. Berg, J. Chisholm, M. Franco, S. L. Finkelstein et al., *Strong rest-uv emission lines in a "little red dot"agn at $\$z=7\$$: Early smbh growth alongside compact massive star formation?*, 2024, <https://api.semanticscholar.org/CorpusID:273026362>.

[132] M. A. Stone, J. Lyu, G. H. Rieke, S. Alberts and K. N. Hainline, *Undermassive Host Galaxies of Five $z \sim 6$ Luminous Quasars Detected with JWST*, *Astrophys. J.* **964** (2024) 90 [2310.18395].

[133] M. Yue, A.-C. Eilers, R. A. Simcoe, R. Mackenzie, J. Matthee, D. Kashino et al., *EIGER. V. Characterizing the Host Galaxies of Luminous Quasars at $z \gtrsim 6$* , *Astrophys. J.* **966** (2024) 176 [2309.04614].

[134] Y. Harikane, Y. Zhang, K. Nakajima, M. Ouchi, Y. Isobe, Y. Ono et al., *A JWST/NIRSpec First Census of Broad-line AGNs at $z = 4-7$: Detection of 10 Faint AGNs with $M_{BH} 10^6-10^8 M_{\odot}$ and Their Host Galaxy Properties*, *Astrophys. J.* **959** (2023) 39 [2303.11946].

[135] X. Ding, M. Onoue, J. D. Silverman, Y. Matsuoka, T. Izumi, M. A. Strauss et al., *Detection of stellar light from quasar host galaxies at redshifts above 6*, *Nature* **621** (2022) 51.

[136] I. Juodzbalis, R. Maiolino, W. M. Baker, S. Tacchella, J. Scholtz, F. D'Eugenio et al., *A dormant overmassive black hole in the early Universe*, *Nature (London)* **636** (2024) 594 [2403.03872].

[137] E. Salpeter, *Accretion of interstellar matter by massive objects.*, *The Astrophysical Journal* **140** (1964) 796.

[138] S. L. Shapiro, *Spin, accretion and the cosmological growth of supermassive black holes*, *Astrophys. J.* **620** (2005) 59 [astro-ph/0411156].

[139] J. F. Navarro, C. S. Frenk and S. D. M. White, *The Structure of cold dark matter halos*, *Astrophys. J.* **462** (1996) 563 [astro-ph/9508025].

[140] J. F. Navarro, C. S. Frenk and S. D. M. White, *A Universal density profile from hierarchical clustering*, *Astrophys. J.* **490** (1997) 493 [astro-ph/9611107].

[141] A. Klypin, A. V. Kravtsov, J. Bullock and J. Primack, *Resolving the structure of cold dark matter halos*, *Astrophys. J.* **554** (2001) 903 [astro-ph/0006343].

[142] B. Moore, T. R. Quinn, F. Governato, J. Stadel and G. Lake, *Cold collapse and the core catastrophe*, *Mon. Not. Roy. Astron. Soc.* **310** (1999) 1147 [astro-ph/9903164].

[143] C. A. Correia, J. S. B. Wyithe, J. Schaye and A. R. Duffy, *The accretion history of dark matter haloes – III. A physical model for the concentration–mass relation*, *Mon. Not. Roy. Astron. Soc.* **452** (2015) 1217 [1502.00391].

[144] O. Fakhouri, C.-P. Ma and M. Boylan-Kolchin, *The Merger Rates and Mass Assembly Histories of Dark Matter Haloes in the Two Millennium Simulations*, *Mon. Not. Roy. Astron. Soc.* **406** (2010) 2267 [1001.2304].

[145] P. S. Behroozi, "Universemachine data release 1 + neutraluniversemachine (jwst lightcones, observational constraints, halo catalogs, merger trees, . . .)." <https://www.peterbehroozi.com/data.html>, 2019.

[146] S. Murray, C. Power and A. S. G. Robotham, *HMFcalc: An online tool for calculating dark matter halo mass functions*, *Astron. Comput.* **3-4** (2013) 23 [1306.6721].

[147] S. Murray, "HMF: Halo Mass Function calculator." Astrophysics Source Code Library, record ascl:1412.006,

Dec., 2014.

[148] A.-C. Eilers, J. F. Hennawi, F. B. Davies and R. A. Simcoe, *Detecting and Characterizing Young Quasars II: Four Quasars at $z \sim 6$ with Lifetimes $< 10^4$ years*, [2106.04586](#).

[149] E. Pizzati et al., *A unified model for the clustering of quasars and galaxies at $z \approx 6$* , *Mon. Not. Roy. Astron. Soc.* **534** (2024) 3155 [[2403.12140](#)].

[150] J. Wu et al., *Demographics of $z \sim 6$ quasars in the black hole mass-luminosity plane*, *Mon. Not. Roy. Astron. Soc.* **517** (2022) 2659 [[2210.02518](#)].

[151] V. Kokorev, K. I. Caputi, J. E. Greene, P. Dayal, M. Trebitsch, S. E. Cutler et al., *A census of photometrically selected little red dots at $4 \leq z \leq 9$ in jwst blank fields*, *The Astrophysical Journal* **968** (2024) 38.

[152] A. J. Taylor, S. L. Finkelstein, D. D. Kocevski, J. Jeon, V. Bromm, R. O. Amorín et al., *Broad-line agns at $3.5 \leq z \leq 6$: The black hole mass function and a connection with little red dots*, *The Astrophysical Journal* **986** (2025) 165.

[153] S. Khan, S. Husa, M. Hannam, F. Ohme, M. Pürrer, X. Jiménez Forteza et al., *Frequency-domain gravitational waves from nonprecessing black-hole binaries. II. A phenomenological model for the advanced detector era*, *Phys. Rev. D* **93** (2016) 044007 [[1508.07253](#)].

[154] S. Husa, S. Khan, M. Hannam, M. Pürrer, F. Ohme, X. Jiménez Forteza et al., *Frequency-domain gravitational waves from nonprecessing black-hole binaries. I. New numerical waveforms and anatomy of the signal*, *Phys. Rev. D* **93** (2016) 044006 [[1508.07250](#)].

[155] A. Nitz, I. Harry, D. Brown, C. M. Biwer, J. Willis, T. D. Canton et al., *gwastro/pycbc: v2.3.3 release of pycbc*, 2024. 10.5281/ZENODO.10473621.

[156] T. Robson, N. J. Cornish and C. Liu, *The construction and use of LISA sensitivity curves*, *Class. Quant. Grav.* **36** (2019) 105011 [[1803.01944](#)].

[157] T. Robson, N. Cornish and L. Chang, “LISA Sensitivity Calculator (2018).” https://github.com/extremeGravityInstitute/LISA_Sensitivity, July, 2019.

[158] A. Sesana et al., *Unveiling the gravitational universe at μ -Hz frequencies*, *Exper. Astron.* **51** (2021) 1333 [[1908.11391](#)].

[159] E. S. Phinney, *A Practical theorem on gravitational wave backgrounds*, [astro-ph/0108028](#).

[160] I. Jaroschewski, J. Becker Tjus and P. L. Biermann, *Extragalactic neutrino-emission induced by supermassive and stellar mass black hole mergers*, *Mon. Not. Roy. Astron. Soc.* **518** (2022) 6158 [[2210.11337](#)].

[161] P. C. Peters, *Gravitational Radiation and the Motion of Two Point Masses*, *Phys. Rev.* **136** (1964) B1224.

[162] L. A. Gergely and P. L. Biermann, *The Spin-Flip Phenomenon in Supermassive Black hole binary mergers*, *Astrophys. J.* **697** (2009) 1621 [[0704.1968](#)].

[163] A. Sesana, C. Roedig, M. T. Reynolds and M. Dotti, *Multimessenger astronomy with pulsar timing and X-ray observations of massive black hole binaries*, *Mon. Not. Roy. Astron. Soc.* **420** (2012) 860 [[1107.2927](#)].

[164] A. Cavaliere, M. Tavani, P. Munar-Adrover and A. Argan, *Supermassive Binaries in Quasars and BL Lac Objects: Electromagnetic and Gravitational Wave Emissions*, *Astrophys. J. Lett.* **875** (2019) L22.

[165] EPTA, InPTA: collaboration, *The second data release from the European Pulsar Timing Array - III. Search for gravitational wave signals*, *Astron. Astrophys.* **678** (2023) A50 [[2306.16214](#)].

[166] D. J. Reardon et al., *Search for an Isotropic Gravitational-wave Background with the Parkes Pulsar Timing Array*, *Astrophys. J. Lett.* **951** (2023) L6 [[2306.16215](#)].

[167] G. Collaboration, *The gaia mission*, 2016, <https://api.semanticscholar.org/CorpusID:119229059>.

[168] G. Janssen et al., *Gravitational wave astronomy with the SKA*, *PoS AASKA14* (2015) 037 [[1501.00127](#)].

[169] A. Sesana and D. G. Figueroa, *Nanohertz Gravitational Waves*, [2512.18822](#).

[170] W. H. Press and D. N. Spergel, *Capture by the sun of a galactic population of weakly interacting massive particles*, *Astrophys. J.* **296** (1985) 679.

[171] A. Gould, *Resonant Enhancements in WIMP Capture by the Earth*, *Astrophys. J.* **321** (1987) 571.

[172] A. Gould, *Resonant Enhancements in Weakly Interacting Massive Particle Capture by the Earth*, *Astrophys. J.* **321** (1987) 571.

[173] I. Goldman and S. Nussinov, *Weakly Interacting Massive Particles and Neutron Stars*, *Phys. Rev. D* **40** (1989) 3221.

[174] B. Dasgupta, A. Gupta and A. Ray, *Dark matter capture in celestial objects: Improved treatment of multiple scattering and updated constraints from white dwarfs*, *JCAP* **08** (2019) 018 [[1906.04204](#)].

[175] B. Dasgupta, A. Gupta and A. Ray, *Dark matter capture in celestial objects: light mediators, self-interactions, and complementarity with direct detection*, *JCAP* **10** (2020) 023 [[2006.10773](#)].

[176] T. N. Maity and F. S. Queiroz, *Detecting bosonic dark matter with neutron stars*, *Phys. Rev. D* **104** (2021) 083019 [[2104.02700](#)].

[177] D. Bose, T. N. Maity and T. S. Ray, *Neutrinos from captured dark matter annihilation in a galactic population of neutron stars*, *JCAP* **05** (2022) 001 [[2108.12420](#)].

[178] J. Bramante, B. J. Kavanagh and N. Raj, *Scattering Searches for Dark Matter in Subhalos: Neutron Stars, Cosmic Rays, and Old Rocks*, *Phys. Rev. Lett.* **128** (2022) 231801 [[2109.04582](#)].

[179] D. Bose, T. N. Maity and T. S. Ray, *Solar constraints on captured electrophilic dark matter*, *Phys. Rev. D* **105** (2022) 123013 [[2112.08286](#)].

[180] M. Baryakhtar et al., *Dark Matter In Extreme Astrophysical Environments*, in *Snowmass 2021*, 3, 2022, [2203.07984](#).

[181] A. Ray, *Celestial objects as strongly-interacting nonannihilating dark matter detectors*, *Phys. Rev. D* **107** (2023) 083012 [[2301.03625](#)].

[182] J. Bramante and N. Raj, *Dark matter in compact stars*, *Phys. Rept.* **1052** (2024) 1 [[2307.14435](#)].

[183] T. N. Maity, A. K. Saha, S. Mondal and R. Laha, *Neutrinos from the Sun can discover dark matter-electron scattering*, *Phys. Rev. D* **112** (2025) 023025 [[2308.12336](#)].

[184] D. Bose, D. Chowdhury, P. Mondal and T. S. Ray, *Troubles mounting for multipolar dark matter*, *JHEP* **06** (2024) 014 [[2312.05131](#)].

[185] D. Bose, R. Pramanick and T. S. Ray, *Neutrinos from captured dark matter in galactic stars*, *Phys. Lett. B*

866 (2025) 139542 [[2405.07894](#)].

[186] D. Krishna, R. Sherpa, A. K. Saha, T. N. Maity, R. Laha and N. Raj, *ν limits from Super-Kamiokande on dark matter-electron scattering in the Sun*, [2503.07713](#).

[187] A. Bhutani, N. Raj and Z. Zuraiq, *Dark, deep, deconfining: Phase transitions in neutron stars as powerful probes of hidden sectors*, [2507.08076](#).

[188] Y. Liu, Z. Liu, M. Pospelov and S. Reddy, *Constraints on Symmetric Dark Matter from Neutron Star Capture and Collapse*, [2508.04961](#).

[189] A. K. Saha, A. Dubey and N. Raj, *Hawking heating of neutron stars by dark matter*, [2511.19599](#).

[190] S. Bhattacharya, S. Kapadia and B. Dasgupta, *Distinguishing Neutron Star vs. Low-Mass Black Hole Binaries with Postmerger Gravitational Waves – Sensitivity to Transmuted Black Holes and Non-Annihilating Dark Matter*, [2507.15951](#).

[191] D. Bose and S. Sarkar, *Impact of galactic distributions in celestial capture of dark matter*, *Phys. Rev. D* **107** (2023) 063010 [[2211.16982](#)].

[192] R. Schneider, *Constraining the epoch of very massive star formation*, *New Astronomy Reviews* **50** (2006) 64.

[193] S. D. McDermott, H.-B. Yu and K. M. Zurek, *Constraints on Scalar Asymmetric Dark Matter from Black Hole Formation in Neutron Stars*, *Phys. Rev. D* **85** (2012) 023519 [[1103.5472](#)].

[194] B. Dasgupta, R. Laha and A. Ray, *Low Mass Black Holes from Dark Core Collapse*, *Phys. Rev. Lett.* **126** (2021) 141105 [[2009.01825](#)].

[195] S. Bhattacharya, B. Dasgupta, R. Laha and A. Ray, *Can LIGO Detect Nonannihilating Dark Matter?*, *Phys. Rev. Lett.* **131** (2023) 091401 [[2302.07898](#)].

[196] S. Bhattacharya, A. L. Miller and A. Ray, *Continuous gravitational waves: A new window to look for heavy nonannihilating dark matter*, *Phys. Rev. D* **110** (2024) 043006 [[2403.13886](#)].

[197] XENON collaboration, *Light Dark Matter Search with Ionization Signals in XENON1T*, *Phys. Rev. Lett.* **123** (2019) 251801 [[1907.11485](#)].

[198] F. C. van den Bosch, B. E. Robertson, J. J. Dalcanton and W. J. G. de Blok, *Constraints on the structure of dark matter halos from the rotation curves of low surface brightness galaxies*, *Astron. J.* **119** (2000) 1579 [[astro-ph/9911372](#)].

Dark Recipe for the First Giants: From Population III Stars to Early Supermassive Black Holes via Dark Matter Capture

Supplemental Material

Sulagna Bhattacharya, Debajit Bose, Basudeb Dasgupta, Jaya Doliya, and Ranjan Laha

S1. DM CAPTURE

In the early Universe, DM halos of masses $\gtrsim 10^5$ – 10^6 M_⊙ are expected to harbor Pop III stars. While a star hovers through the sea of DM particles, the stellar gravitational potential focuses the DM particles toward the star. If the DM particles share non-gravitational interactions with SM states, they can scatter with stellar constituents and lose sufficient energy to become bound to the star [170–172]. DM capture in celestial bodies can result in a broad class of observable signatures, which have been studied in [173–190]. The capture rate of DM particles inside the Pop III stars is

$$C_\chi = \pi R_s^2 \left(\frac{\rho_\chi}{m_\chi} \right) \int d^3 u_\chi \frac{f(\vec{u}_\chi)}{u_\chi} (u_\chi^2 + v_{\text{esc}}^2) P_{\text{cap}}, \quad (\text{S1})$$

where R_s is the radius of the Pop III star, m_χ and u_χ are the mass and ambient velocity of the DM particles, respectively, and ρ_χ is the DM density in the vicinity of the Pop III star. In Eq. S1, the velocity distribution profile is taken to be a Maxwell-Boltzmann distribution ($f(\vec{u}_\chi)$)¹ boosted to the rest frame of the star, v_{esc} is the escape velocity of the star and $P_{\text{cap}} = \Theta(v_{\text{max}} - u_\chi)$ is the capture probability of the DM particle with velocity u_χ and v_{max} is [102]

$$v_{\text{max}} = \begin{cases} v_{\text{esc}} \left[\left(1 - \frac{\beta_+}{2} \right)^{-n_{\text{coll}}} - 1 \right]^{1/2} & ; m_\chi u_\chi^2 \gg m_k v_k^2, \\ v_k \sqrt{2n_{\text{coll}}} \left(\frac{m_k}{m_\chi + m_k} \right) & ; m_\chi u_\chi^2 \ll m_k v_k^2, \end{cases} \quad (\text{S2})$$

where the target particle mass is denoted by m_k , and the kinematic parameter $\beta_+ = 4m_\chi m_k / (m_\chi + m_k)^2$. The velocity of the target particle (v_k) is obtained from the relation $\frac{3}{2}k_B T_s = \frac{1}{2}m_k v_k^2$, with T_s denoting the stellar temperature, k_B is the Boltzmann constant. In Eq. S2, $n_{\text{coll}} = R_s \rho_s \sigma_{\chi k} / m_k$ is the average number of collisions a DM particle encounters while traversing the star, and $\sigma_{\chi k}$ is the scattering cross-section of DM with the target particle. In the parameter space relevant for our analysis, i.e., $m_\chi v_{\text{esc}}^2 \gg m_k v_k^2$, the mass capture rate for $M_s = 100$ M_⊙ and $R_s = 6$ R_⊙ can be described by the approximate expression

$$m_\chi C_\chi|_{\text{approx}} = 6.85 \times 10^{-16} \times \left(\frac{\rho_\chi}{10^{11} \text{ GeV/cm}^3} \right) \times \left(\frac{200 \text{ GeV}}{m_\chi} \right) \times \left(\frac{\sigma_{\chi k}}{9.25 \times 10^{-43} \text{ cm}^2} \right) \text{ M}_\odot/\text{s} \quad (\text{S3})$$

where the velocity dispersion is taken to be $v_d = 5$ km/s. For our analysis, we compute the capture rate using Eq. S1 incorporating the stellar properties of Pop III stars, and we check that for $m_\chi = 200$ GeV and $\sigma_{\chi p}^{\text{SD}} = 9.25 \times 10^{-43} \text{ cm}^2$, the capture rates obtained from Eq. S1 and S3 differ by a factor of 3.35. We have extracted the stellar properties by simulating the Pop III stars with Modules for Experiments in Stellar Astrophysics (MESA) [116–121] with an initial metallicity of 10^{-12} , consistent with [192]. We track the central hydrogen mass fraction (X_c) from the `history.data` file to extract details of the stellar interior. When the hydrogen fraction $X_c \lesssim 0.6$, we extract the corresponding `profile.data` file to obtain the stellar profile at that epoch. The value of X_c is chosen to be ~ 0.6 to ensure that the Pop III stars remain within the main sequence phase of their lives. We extract the stellar radius, density, and temperature profiles from the output profile. The radial density and temperature profiles of Pop III stars are shown in Fig. S1 for some representative stellar masses. To compute the mean density and temperature, we evaluate the average over all radial grid points provided in the output profile.

¹ Possible deviations and their effects are studied in [191].

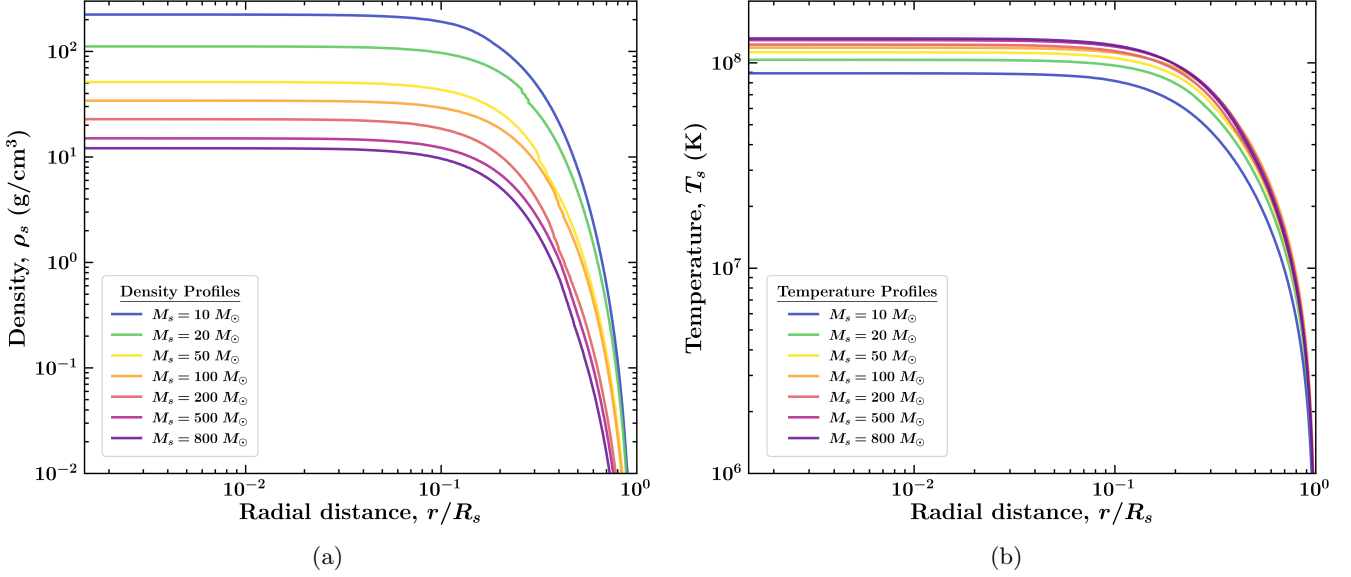


FIG. S1: The density (left) and temperature (right) profiles as a function of radial distance, obtained using MESA, are shown for Pop III stars with masses ranging from $10 M_{\odot}$ to $800 M_{\odot}$.

S2. IMPORTANT TIMESCALES

A. Thermalization timescale

After being captured by Pop III stars, the DM particles initially become bound on orbits with semi-major axes larger than the stellar radius (R_s), so their trajectories pass through the star. During each passage, the DM scatters with SM particles in the stellar medium and loses energy. If the velocity of DM after scattering becomes $v_{\text{final}} = v_{\text{esc}}(1 - \xi)$, the total time required for the orbit to be entirely inside the star is [102]

$$\tau_{\text{therm},a} = \frac{\pi}{\sqrt{2}v_{\text{esc}}\rho_s\sigma_{\chi k}} \begin{cases} m_{\chi} \left(\frac{1}{\sqrt{\xi(2-\xi)}} - 1 + \frac{\tanh^{-1}(\sqrt{2}) - \tanh^{-1}\left(\frac{\sqrt{2}}{\sqrt{\xi(2-\xi)}}\right)}{\sqrt{2}} \right); m_{\chi}v_{\text{esc}}^2 \gg m_k v_k^2 \\ m_k \frac{v_{\text{esc}}^2}{v_k^2} \left(\frac{1}{\sqrt{\xi(2-\xi)}} - 1 \right); m_{\chi}v_{\text{esc}}^2 \ll m_k v_k^2. \end{cases} \quad (\text{S4})$$

After the DM orbits are confined within the stellar interior, they keep scattering with the stellar constituents and lose energy. Thus, with sufficient scatterings, the DM particles settle into the core and attain a velocity corresponding to the ambient stellar temperature, which marks the completion of the thermalization stage. The time required for the DM to drift from the outer envelope to the core of the star can be expressed as [102]

$$\tau_{\text{therm},b} = \begin{cases} \frac{m_{\chi} \log\left(\frac{2Gm_{\chi}M_s}{3R_sT_s}\right)}{4\rho_{s,c}\sigma_{\chi k}c_s}; & m_{\chi} \gg m_k \\ \frac{m_k^2 \log(2)}{4\rho_{s,c}\sigma_{\chi k}c_s m_{\chi}} + \frac{m_k \left(\log(2) + \frac{GM_s}{c_s^2 R_s} \right)}{\rho_{s,c}\sigma_{\chi k}c_s}; & m_{\chi} \ll m_k \end{cases} \quad (\text{S5})$$

where $\rho_{s,c}$ denotes the density of the stellar core and c_s is the sound speed within the stellar medium, which is taken to be $c_s \sim v_k$. As mentioned earlier (Fig. S1), the Pop III stars have been simulated using MESA and the corresponding stellar properties have been extracted by combining the `history.data` and `profile.data` files. As described in Eq. S4

and S5, the total thermalization time is defined as the total time the DM particles need to form a thermalized core from the outer orbits, i.e., $\tau_{\text{therm}} = \tau_{\text{therm},a} + \tau_{\text{therm},b}$.

B. Collapse timescale

For our parameter space of interest, the BH formation is triggered by the self-gravity criterion (irrespective of whether the DM is a boson or a fermion), i.e., $\rho_{\chi,c} \gg \rho_{s,c}$ with $\rho_{\chi,c}$ being the accumulated DM density at the stellar core [113, 193–196]. Once this criterion is satisfied, the time required for the thermalized radius r_{therm} to contract to the Schwarzschild radius r_{Sch} is [102]

$$\tau_{\text{col}} = \frac{1}{4\rho_{s,c}c_s\sigma_{\chi k}} \begin{cases} m_\chi \log\left(\frac{c_s^2 r_{\text{therm}}}{GM_{\text{Self}}}\right); & m_\chi \gg m_k \\ m_k \left(\frac{\sqrt{2}}{c_s} - \frac{2}{c_s} \sqrt{\frac{GM_{\text{Self}}}{r_{\text{therm}}}} + \log\left(\frac{r_{\text{therm}}}{2GM_{\text{Self}}}\right) \right); & m_\chi \ll m_k \end{cases} \quad (\text{S6})$$

where the thermalized radius is obtained by balancing the thermal energy and gravitational potential in the stellar core, i.e., $r_{\text{therm}} = \sqrt{9T_s/4\pi G\rho_{s,c}m_\chi}$.

C. Bondi accretion timescale

After the tiny BH is formed at the heart of a Pop III star, it starts accreting the stellar material and emitting Hawking radiation. As shown in [102], for a typical Pop III star with a mass $\mathcal{O}(100)M_\odot$, Hawking radiation dominates only if the DM mass is close to the Planck scale. The DM is much lighter in our scenario, so Hawking radiation can be safely neglected. Although Pop III stars will continue to capture additional DM, we ignore this effect and focus solely on accretion. We model this process using Bondi accretion [115], which applies to non-rotating, uncharged BHs. The timescale for the tiny BH to consume the entire star and form a stellar-mass BH is

$$\tau_{\text{Bondi}} = \frac{c_s^3}{4\pi\alpha G^2\rho_{s,c}} \left(\frac{1}{M_{\text{Self}}} - \frac{1}{M_s} \right), \quad (\text{S7})$$

where $\alpha \sim 1$ [115], and M_s and M_{Self} are the mass of the star and self-gravitating mass, respectively. In Table S1, we show the specific timescales to form the seed BH from $100 M_\odot$ Pop III star, for our benchmark point ($m_\chi = 200 \text{ GeV}$, $\sigma_{\chi p}^{\text{SD}} = 9 \times 10^{-43} \text{ cm}^2$) used in this study. Within our parameter space of interest, the thermalization timescale dominates and governs the seed BH formation time.

Timescales	in yrs
τ_{accum}	8.8×10^{-1}
τ_{therm}	1.5×10^5
τ_{col}	2×10^3
τ_{Bondi}	3×10^{-3}
τ	1.5×10^5

TABLE S1: The specific timescales involved in the premature death of a $100 M_\odot$ Pop III star via DM-capture induced transmutation are shown for our benchmark point ($m_\chi = 200 \text{ GeV}$, $\sigma_{\chi p}^{\text{SD}} = 9 \times 10^{-43} \text{ cm}^2$). The last entry of the table, τ , represents the total timescale to form the seed BH as discussed in Eq. 1.

S3. DARK MATTER - ELECTRON SCATTERING

We have also explored our framework for DM capture via its scattering with electrons inside the Pop III stars. To compute the electron mass density inside the stars, we use the proton number density together with the charge neutrality condition. Since the electron mass is much smaller than the proton mass, electrons are semi-relativistic

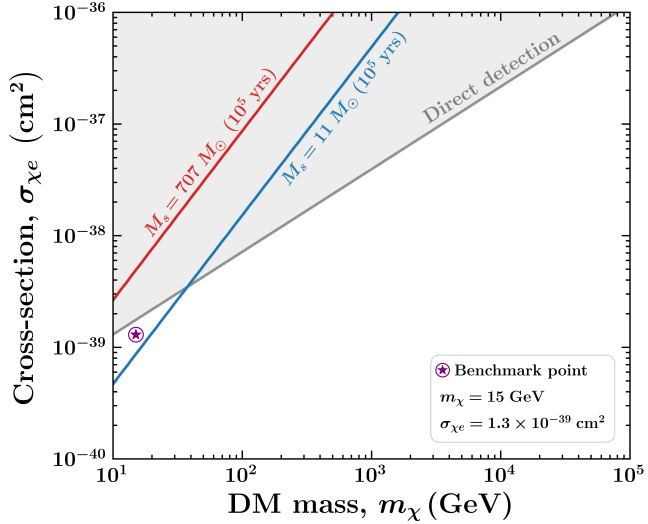


FIG. S2: Contours of BH formation time of 10^5 yr for the lowest and highest mass Pop III stars for DM-electron interaction are shown with blue and red solid lines, respectively [36]. The gray shaded region represents the extended direct detection limits from XENON1T [197]. The purple point denotes the benchmark scenario that evades current constraints and successfully leads to the formation of a seed BH.

in the stellar interior, and their velocities are calculated from the stellar temperature. The equal-time contours for seed BH formation (isochrones) with $\tau = 10^5$ yrs are shown in Fig. S2. The blue and red contours correspond to the lowest ($11 M_\odot$, $1.5 R_\odot$, $\tau_{\text{lifetime}}^{\text{PopIII}} = 14.5$ Myr) and highest Pop III masses ($707 M_\odot$, $16.4 R_\odot$, $\tau_{\text{lifetime}}^{\text{PopIII}} = 1.9$ Myr), respectively [36]. The gray shaded region denotes the direct detection limits from XENON1T [197], extended to higher masses using appropriate scaling. For the DM-electron benchmark point ($m_\chi = 15$ GeV, $\sigma_{\chi e} = 1.3 \times 10^{-39} \text{ cm}^2$), the BH formation timescale (τ) is comparable to that obtained for the benchmark parameters of DM–proton SD interaction. Consequently, all subsequent results are expected to be very similar for the case of DM–electron scattering as well. However, it should be noted that, for higher Pop III masses, the timescale would exceed 10^5 yrs for the considered DM–electron benchmark point, which may lead to noticeable differences in other results.

S4. DARK MATTER HALO

In this work, we adopt a gNFW DM halo profile, which is parametrized as [139–141]

$$\rho_\chi(r) = \frac{\rho_0}{\left(\frac{r}{r_s}\right)^\gamma \left[1 + \left(\frac{r}{r_s}\right)\right]^{3-\gamma}}, \quad (\text{S8})$$

where ρ_0 , r_s are the characteristic density and the scale radius, respectively, and the inner slope is fixed at $\gamma = 3/2$ [142]. However, we have checked that for $\gamma \geq 1.24$, the required density $\rho_\chi = 10^{11} \text{ GeV/cm}^3$ can be reached at distances exceeding 10 times the typical radius of a Pop III star, i.e., $50 R_\odot$. Therefore, our analysis remains valid for gNFW DM profiles with $\gamma \geq 1.24$. We rewrite the density profile so that it is expressed directly in terms of the halo mass (M_{200}) and the concentration parameter (c_{200}). The parameters ρ_0 and r_s are then determined using two conditions: (i) the mean density within r_{200} satisfies $\bar{\rho}(r_{200}) = 200 \rho_{\text{crit}}$, where ρ_{crit} is the critical density of the universe at that epoch and $r_{200} = c_{200} r_s$, and (ii) the enclosed mass within r_{200} is $M_{200} = \int_0^{r_{200}} 4\pi r^2 \rho_\chi(r) dr$. Using this density profile, we determine the radial position in the halo where $\rho_\chi = 10^{11} \text{ GeV}$, i.e., r_{11} , and assume that the Pop III star is located at this position. Our framework is insensitive to the precise location of the Pop III star, and remains valid for any position within the radius r_{11} . We need to estimate the typical halo velocities to calculate the capture rate at that location in the halo. The halo escape velocity at a distance r from the center is $u_{\text{esc}} = \sqrt{-2V(r)}$, where $V(r)$ is the

gravitational potential. We have estimated the halo rotational velocity at the same location using the relation [198]

$$u_{\text{rot}}(r) = \sqrt{\frac{r_{200} v\left(\frac{r c_{200}}{r_{200}}\right)}{r v(c_{200})}}, \quad \text{with } v(y) = \int_0^y x^{2-\gamma} (1+y)^{\gamma-3} dy. \quad (\text{S9})$$

Among the relevant timescales, only the accumulation timescale (τ_{accum}) depends on the DM density profile. As shown in Table S1, τ_{accum} is much smaller than the thermalization timescale (τ_{therm}). We have checked that the total timescale for the benchmark point ($m_\chi = 200 \text{ GeV}$, $\sigma_{\chi p}^{\text{SD}} = 9 \times 10^{-43} \text{ cm}^2$) remains approximately unchanged even when the Pop III star is placed at a location (r_9 , i.e., where $\rho_\chi = 10^9 \text{ GeV/cm}^3$), for which the condition $r_9 = 50 \times R_\odot$ can be achieved even for the NFW profile, i.e., $\gamma = 1$.

In [144], a fitting formula for the halo growth rate as a function of the halo mass and the redshift is provided, considering growth via both accretion and mergers. To model the growth of our halos, we adopt the mean fitting formula expressed as [144]

$$\left\langle \frac{dM_{\text{halo}}}{dt} \right\rangle = 46.1 \left(\frac{M_{\text{halo}}}{10^{12} M_\odot} \right)^{1.1} (1 + 1.11 z) \sqrt{\Omega_m(1+z)^3 + \Omega_\Lambda} \text{ M}_\odot/\text{yr}. \quad (\text{S10})$$

Since the fitting relation is shown only up to $z = 14$ in [144], for redshifts beyond this limit, we keep the halo accretion rate fixed at its maximum value at $z = 14$ instead of allowing it to increase monotonically at higher redshifts.

S5. DETAILED EXPLANATION OF FIGURE 2

A. Black Hole Mass vs Observed Redshift

Fig. 2a represents the observed mass of the BH, formed through DM capture inside Pop III stars, as a function of z_{obs} . Different bands correspond to different accretion rates, η_{acc} , for the evolution of seed BHs. Each band is an envelope of sub-bands that correspond to four different z_{in} values (16, 20, 24, 28). The lower and upper edges of these sub-bands correspond to the lowest and highest mass Pop III stars, respectively, at that z_{in} (see Fig. 17 of [36]). Therefore, the lower and upper edges of the bands in Fig. 2a represent the lowest mass Pop III star (at $z_{\text{in}} = 16$) and the highest mass Pop III star (at $z_{\text{in}} = 28$), respectively. We also plot the observational data and find that most of the observations can be explained by this mechanism.

B. Black Hole Mass vs Stellar Mass

Fig. 2b shows the relation between the BH mass and the host galaxy stellar mass at $z_{\text{obs}} = 6$ for four different seed BH accretion efficiencies, indicated by different colors. We consider halo masses in the range $M_{\text{halo}} \in [10^6, 10^9] M_\odot$. After tracking the halo growth up to z_{obs} with Eq. (S10), we compute the galaxy stellar mass using the fitting relation from Data Release 1 of the UniverseMachine code [145]. Each color contains several sub-bands determined by the initial redshifts of the Pop III stars. For each sub-band, the horizontal width arises from changes in the halo mass, while the vertical width reflects differences in the initial Pop III star mass, taken from [36]. We impose an upper cut on the BH mass of $10^{11} M_\odot$ and on the host galaxy stellar mass of $10^{12} M_\odot$. In addition, we apply the condition $M_{\text{BH}}^{\text{obs}} \leq M_{\text{halo}}^{\text{obs}}$, which deforms the shape of some sub-bands away from being rectangular.

S6. GRAVITATIONAL WAVES

In this section, we will outline the calculation of GW signatures of SMBH mergers. For individual mergers, we compute the gravitational wave amplitudes, $\tilde{h}(f)$, with the pyCBC code [155] and the corresponding sky-averaged LISA SNR is calculated by the formula [156]

$$\text{SNR} = \frac{16}{5} \int_0^\infty df \frac{\left| \tilde{h}(f) df \right|^2}{S_n(f)}, \quad (\text{S11})$$

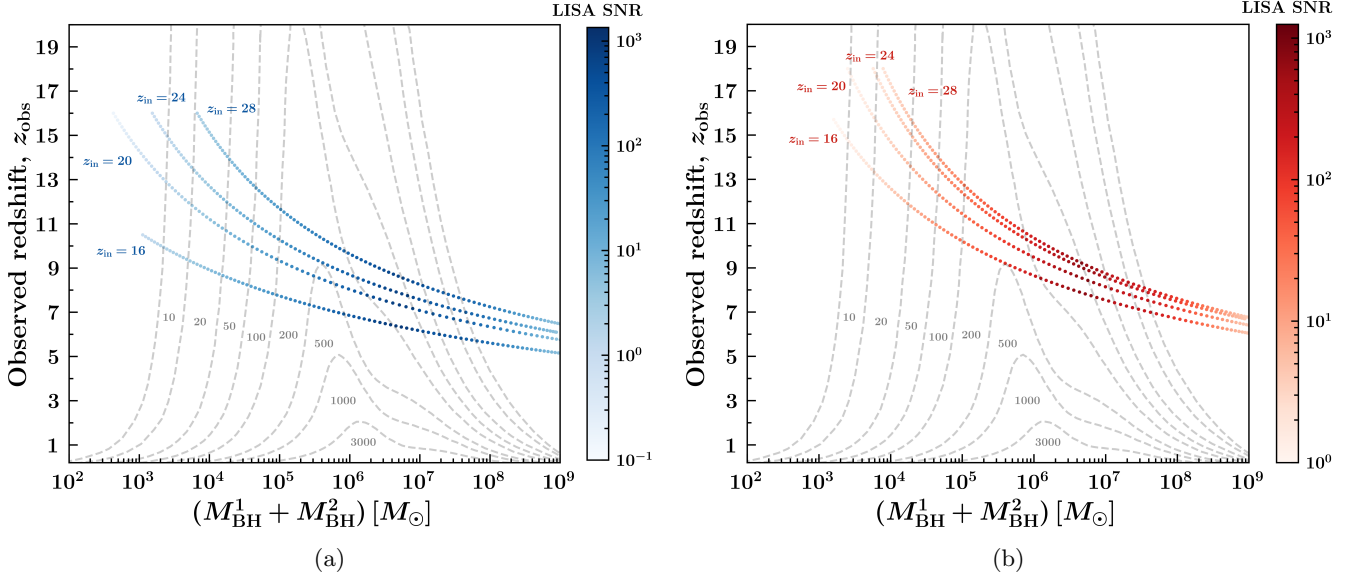


FIG. S3: Color plot of the LISA SNR in the observed redshift and total BH mass plane. The color bars correspond to the SNR values of the lowest (left) and highest (right) Pop III star masses. For each mass case, four distinct tracks represent different initial redshifts ($z_{\text{in}} = 16, 20, 24, 28$). The gray dashed lines indicate contours of constant LISA SNR [104].

where $S_n(f)$ denotes the one-sided power spectral density of detector noise (for LISA) taken from [156]. In Fig. 4, we present the characteristic strain for representative mergers expected in our scenario for the lowest and highest z_{in} . To compute the SNR, we use all four benchmark z_{in} values, i.e., (16, 20, 24, 28), mentioned in the manuscript. After the seed BH forms from a Pop III star with the benchmark SD DM-proton scattering cross-section, we choose the subsequent Eddington accretion of the seed to calculate the SNR of symmetric individual mergers. We scan over the observed redshifts and calculate $h(f)$ using `pyCBC`, incorporating the luminosity distance, to check whether the signal amplitude falls within the LISA sensitivity window. We then compute the SNR for those mergers that have at least partial overlap with the LISA band. In Fig. S3, we show the resulting SNR across the scanned redshifts, considering both the lightest (blue) and the heaviest (red) Pop III star masses in the left and right panels, respectively.

We estimate the GW background using the framework of [160], which is based on [159]. The characteristic strain of the GW background is given by [159, 160]

$$h_{c,\text{back}} = 3 \times 10^{-24} \left(\frac{\mathcal{M}_c}{M_\odot} \right)^{5/6} \left(\frac{f}{1 \text{ mHz}} \right)^{-2/3} \left(\frac{n_{\text{SMBH}}^{\text{merge}}}{\text{Mpc}^{-3}} \right)^{1/2} \left(\frac{\langle (1+z)^{-1/3} \rangle}{0.74} \right)^{1/2}, \quad (\text{S12})$$

where \mathcal{M}_c denotes the chirp mass. For two SMBHs merging with masses M_{BH}^1 and $M_2 = \lambda M_{\text{BH}}^2$, the resulting SMBH mass after the merger can be written as [160]

$$M_{\text{final}} = [1 + \zeta_{\text{acc}} + 0.1 \kappa(\lambda)] (1 + \lambda) M_{\text{BH}}^1, \quad (\text{S13})$$

where $\kappa = \sqrt{\lambda^3/(1+\lambda)^6}$ and ζ_{acc} is the fraction of mass accreted by the SMBHs during the merger, and we have fixed it at a constant value of 0.33 [160]. Thus, the chirp mass in Eq. (S12) is expressed as

$$\mathcal{M}_c = \frac{\kappa(\lambda)}{1 - 0.1 \kappa(\lambda)} \times M_{\text{final}}. \quad (\text{S14})$$

In Eq. (S12), the redshift average $\langle (1+z)^{-1/3} \rangle$ is taken to be 0.8 that is valid for a flat universe. As shown in [159], this value depends only mildly on the number density distribution of the mergers. For the SMBH merger mass ratios, we consider λ to be equal to 1/3 and compute the GW background as described in [160]. We find that for λ equal to 1/3 and 1/30, the corresponding strain amplitudes lie in nearly the same range, and given the uncertainties in the merger timescales, the resulting bands largely overlap. Therefore, we show only the strain for $\lambda = 1/3$ in Fig. 4.